Bifurcation properties of nematic liquid crystals exposed to an electric field: Switchability, bistability, and multistability

L. J. Cummings, C. Cai, and L. Kondic

Phys. Rev. E **88**, 012509 — Published 30 July 2013

DOI: 10.1103/PhysRevE.88.012509

Bifurcation properties of nematic liquid crystals exposed to an electric field: switchability, bistability and multistability

L.J. Cummings, C. Cai, L. Kondic
Department of Mathematical Sciences and Center for Applied Mathematics and Statistics
New Jersey Institute of Technology, Newark, NJ 07102

Bistable Liquid Crystal Displays (LCDs) offer the potential for considerable power savings, compared with conventional (monostable) LCDs. The existence of two (or more) stable field-free states that are optically-distinct means that contrast can be maintained in a display without an externally-applied electric field. An applied field is required only to switch the device from one state to the other, as needed. In this paper we examine the basic physical principles involved in generating multiple stable states, and the switching between these states. We consider a two-dimensional geometry in which variable surface anchoring conditions are used to control the steady-state solutions and we explore how different anchoring conditions can influence the number and type of solutions, and whether or not switching is possible between the states. We find a wide range of possible behaviors, including bistability, tristability and tetrastability, and we investigate how the solution landscape changes as the boundary conditions are tuned.

PACS numbers: 42.70.Df, 61.30.Dk, 61.30.Gd, 61.30.Hn

I. INTRODUCTION

In "e-ink" display technology [1], spherical microcapsules are dispersed in a clear carrier fluid. Each microcapsule contains positively charged white particles and negatively charged black ones, which segregate in a DC electric field. If the electric field direction is reversed, so is the segregation of white and black particles in the microcapsule. Hence, display contrast can be controlled by applying fields of appropriate polarities in different portions of the screen (pixels). Once the field is removed, the particles maintain their segregation within the microcapsule, so that a field is required only to change the state of the display. Thus, e-ink is a bistable technology and uses very little power, giving excellent battery lifetimes.

Most e-readers in current use rely on e-ink technology, but most portable phones, netbooks and music players use conventional Liquid Crystal Display (LCD) technology. This latter has better optical properties, but higher power consumption because it requires continuous application of an electric field. At the simplest level, an LCD pixel comprises a thin layer of nematic liquid crystal (NLC) sandwiched between two glass plates, and placed between crossed polarizers. The NLC is birefringent: depending on its internal molecular orientation, it can rotate the plane of polarized light. The molecular orientation can be controlled by boundary effects (so-called *surface anchoring*; depending on how a surface is prepared the NLC molecules have a preferred orientation there), and by application of an electric field across the layer (its typically rod-like molecules align in an applied field). With the molecules aligned, the polarized light that passed through the first polarizer is not rotated as it passes through the NLC layer, and is blocked by the second, crossed, polarizer. With no applied field, however, the molecular orientation within the layer is different (dictated solely by anchoring now, rather than the electric field); the polarized light is rotated as it passes through the NLC layer, and can pass through the second crossed polarizer. These two states are therefore optically-distinct when light is passed through (the first will be dark, the second bright), and form the basis of an LCD. However, since the electric field must be "on" to maintain the contrast between neighboring pixels, such displays are energetically expensive.

One possible way to reduce the power consumption of an LCD device is to design it so that it is bistable, with two stable states for the molecular orientation in the absence of an applied electric field. Provided these stable states are optically-distinct, and may be switched from one to the other by *transient* application of an electric field, power consumption could rival that of e-ink technology, yet with superior optical properties. With no applied field the only way to control the molecular orientation within the device is by surface anchoring effects; hence to achieve bistability, control of surface anchoring is key. If anchoring conditions are chosen appropriately it is found that two (or more) steady states exist for the molecular orientation, and that one can switch reversibly between the two states by applying an electric field across the bounding plates for a few milliseconds (see [2] and §IV in the present paper).

In this paper we investigate theoretically a two dimensional (2D) bistable LCD configuration that generalizes an earlier 1D model [2]. The 1D model considered a simple nematic sandwich between parallel bounding plates, and relied on the premise that the bounding surfaces can be prepared so as to control the preferred molecular orientation of the nematic molecules (the anchoring angle) and the associated anchoring strengths, both being constant on each boundary. Here we consider a scenario in which anchoring properties (specifically, the anchoring angles) vary periodically along the bounding surfaces. This may be thought of as either a true variation in anchoring angle, due (e.g.) to chemical gradients along the flat bounding surfaces; or perhaps more realistically as an approximation to the anchoring variation induced by a periodically-varying surface topography (as in, e.g., the Zenithal Bistable Device, or ZBD [3]). We can view this problem as a perturbation to the associated 1D problem: the anchoring angles are of the form $\alpha = \alpha^{(0)} + \delta\cos(2\pi x^*/L^*)$ where $\alpha^{(0)}$ is the constant anchoring angle in the 1D problem, x^* is the coordinate parallel to the bounding surfaces, L^* is the wavelength of the anchoring variation, and δ is the amplitude, which will play the role of a bifurcation parameter.

The paper is laid out as follows: in §II we introduce the key dependent variables, and outline the basic mathematical model in §§II A, II B. Section II C recaps the results of bistability and switching for the 1D model, presenting the full range of parameter space within which two-way switching is found. Section IV describes briefly the numerical approach taken, and presents our key results. Finally in §V we draw our conclusions.

II. MATHEMATICAL MODEL

The basic setup is a layer of nematic liquid crystal (NLC), sandwiched between parallel bounding surfaces at $z^* = 0$ and $z^* = h^*$. Star superscripts will be used throughout to denote dimensional quantities, and will be dropped when we nondimensionalize. The molecules of the NLC are rod-like, which imparts anisotropy. The molecules like to align locally, which is modeled by associating an elastic energy with any deviations from uniform alignment (§II A below). The local average molecular orientation is described by a director field $\boldsymbol{n}$, a unit vector which, in our 2D model, is confined to the (x^*, z^*)-plane, see Fig. 1. It may therefore be expressed in terms of a single angle $\theta(x^*, z^*, t^*)$,

$$\boldsymbol{n} = (\sin\theta, 0, \cos\theta), \tag{1}$$

where t^* is time. We further assume that the electric field, when applied, is uniform throughout the NLC layer: $\boldsymbol{E}^* = E^*(t^*)(0, 0, 1)$. In reality the electric field and the NLC interact, so that even if $\boldsymbol{E}^*$ is uniform outside the layer, it will vary across the layer. A more careful treatment would take this into account; however, based on a preliminary investigation into variable field effects within a 1D device [4] we do not expect deviations from uniformity to be significant under normal operating conditions, and we expect the uniform field assumption is sufficient for the proof-of-principle investigation here. We recall that in any case an electric field is utilized only to switch the nematic configuration from one state to the other, and therefore the detailed properties of the field are not so important.

Since we require bistability in the absence of an applied field, anchoring conditions at the bounding surfaces $z^* = 0, h^*$ are key. The anchoring pretilt angle (denoted by α in our model, the preferred value of θ at either interface) may be controlled by a variety of surface treatments; for example, mechanical or chemical treatments, nano-patterning, and surface irradiation, have all been shown to produce certain desired anchoring angles [5–17] with a high degree of control. The anchoring strength A^* may also be controlled to some extent [9, 11, 13, 14] by similar methods. As evidenced by these cited works, advances in the degree of control attainable are continually being made and, while not quite yet a reality, "bespoke surfaces" with desired anchoring properties are a real possibility for the near future. We shall therefore assume that surface anchoring angles and strengths are adjustable parameters, within a range of physically-realistic values. We shall furthermore allow the anchoring angles to vary sinusoidally about some average value:

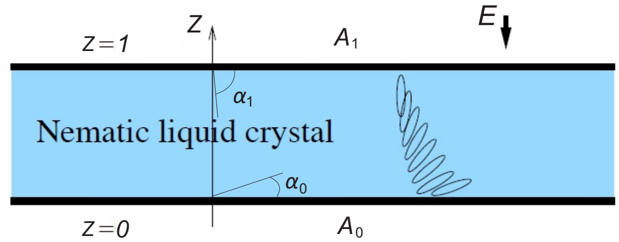

FIG. 1: Sketch showing the setup and summarizing the key parameters in the dimensionless coordinates.

$$\alpha_i = \alpha_i^{(0)} + \delta_i\cos(2\pi x^*/L^* + \phi_i) \quad i = 0, 1, \tag{2}$$
$$\phi_0 = 0,\ \phi_1 \in [0, \pi/2]$$

where $i = 0, 1$ denotes the lower/upper bounding surface, respectively, and $\phi_1 \neq 0$ allows for a phase difference between the variations on each surface. We expect that such periodic variation will approximate the situation in which the bounding surfaces themselves have periodically-varying topography (possibly with a phase difference between upper and lower surfaces) as seen, for example, in the Zenithal Bistable Device (ZBD) or Post Aligned Bistable Device (PABD) [3, 18]. We consider two cases for the amplitude parameters δ_0, δ_1: (i) they take the same value, $\delta_1 = \delta_0 = \delta$, or (ii) $\delta_1 = 0$, $\delta_0 = \delta$ (perturbation only on the lower boundary). Clearly, Eq.(2) is not the most general form of periodic anchoring variation that could be considered; nonetheless we expect the results obtained as δ and L^* are varied to be representative of the more general case, and in the interests of keeping the investigation manageable we restrict attention to this set of perturbations.

A. Energetics

The free energy of the liquid crystal layer, in the presence of an applied electric field and with specified anchoring conditions at each bounding surface, has several contributions. The bulk free energy density consists of elastic, dielectric and flexoelectric contributions W_e^*, W_d^*,

W_f^*, and in our 2D model with the uniform field assumption these are given by

$$2W_e^* = K_1^*(\nabla^* \cdot \boldsymbol{n})^2 + K_3^*((\nabla^* \times \boldsymbol{n}) \times \boldsymbol{n})^2,$$
$$2W_d^* = -\varepsilon_0^*(\varepsilon_\parallel - \varepsilon_\perp)(\boldsymbol{n} \cdot \boldsymbol{E}^*)^2,$$
$$W_f^* = -\boldsymbol{E}^* \cdot (e_1^*(\nabla^* \cdot \boldsymbol{n})\boldsymbol{n} + e_3^*(\nabla^* \times \boldsymbol{n}) \times \boldsymbol{n}),$$

where K_1^* and K_3^* are elastic constants, ε_0^* is the permittivity of free space, $\varepsilon_\parallel$ and $\varepsilon_\perp$ are the relative dielectric permittivities parallel and perpendicular to the long axis of the nematic molecules, and e_1^* and e_3^* are flexoelectric constants [19–21]. With the director field $\boldsymbol{n}$ as given by Eq. (1), and the common simplifying assumption $K_1^* = K_3^* = K^*$, the total bulk free energy density $W^* = W_e^* + W_d^* + W_f^*$ simplifies. Introducing the nondimensional forms $W = K^* W^*/h^{*2}$ and $(x, z) = (x^*, z^*)/h^*$,

$$W = \frac{1}{2}(\theta_x^2 + \theta_z^2) - \mathcal{D}\cos^2\theta + \frac{\mathcal{F}}{2}(\theta_z \sin 2\theta - \theta_x \cos 2\theta) \quad (3)$$

where

$$\mathcal{D} = \frac{h^{*2}E^{*2}\varepsilon_0^*(\varepsilon_\parallel - \varepsilon_\perp)}{2K^*}, \quad \mathcal{F} = \frac{h^* E^*(e_1^* + e_3^*)}{K^*} \quad (4)$$

are dimensionless constants. With representative characteristic values $h^* \sim 2\mu$m, $E^* \sim 1$Vμm^{-1}, $e_1^* + e_3^* \sim 5 \times 10^{-11}$C m^{-1}, $K^* \sim 1 \times 10^{-11}$N, $\varepsilon_\parallel - \varepsilon_\perp \sim 5$, [22–24] both $\mathcal{D}$ and $\mathcal{F}$ are $O(1)$. We emphasize that these values are *not* intended to be absolute; a fair degree of variation about these values is possible, and indeed, many different combinations of dimensional parameter values will lead to the same model in dimensionless form. Note that $\mathcal{D}$ and $\mathcal{F}$ are not independent; the ratio

$$\Upsilon = \frac{\mathcal{F}^2}{\mathcal{D}} = \frac{2(e_1^* + e_3^*)^2}{K^*\varepsilon_0^*(\varepsilon_\parallel - \varepsilon_\perp)} \quad (5)$$

is a material parameter, independent of the geometry. We consider the most common case in which the dielectric anisotropy $\varepsilon_\parallel - \varepsilon_\perp > 0$ (molecules align parallel, rather than perpendicular, to an applied field), so that $\mathcal{D} > 0$ always. The parameter $\mathcal{F}$ characterizing the dimensionless strength of the applied electric field will, however, change sign if the electric field direction is reversed. Since the representative parameter values listed above give $\Upsilon \approx 10$, we assign this value to Υ throughout our computations.

The surface anchoring is modeled by a Rapini-Papoular form [25]; if $g^*_{\{0,h^*\}} = (K^*/h^*)g_{\{0,1\}}$ are the surface energies per unit length at the boundaries $z^* = 0$, h^*, then

$$g_{0,1} = \frac{\mathcal{A}_{\{0,1\}}}{2}\sin^2(\theta - \alpha_{\{0,1\}}), \quad \mathcal{A}_{\{0,1\}} = \frac{h^* A^*_{\{0,h^*\}}}{K^*} \quad (6)$$

where $A^*_{\{0,h^*\}}$ are the anchoring strengths at $z^* = 0$, h^* and $\alpha_{\{0,1\}}$ are the preferred angles, given by Eq. (2): in dimensionless form,

$$\alpha_i = \alpha_i^{(0)} + \delta_i \cos(2\pi x/L + \phi_i) \quad i = 0, 1, \quad (7)$$
$$\phi_0 = 0,\ \phi_1 \in [0, \pi/2]$$

where the dimensionless perturbation wavelength $L = L^*/h^*$. As $\mathcal{A} \to \infty$ the anchoring becomes strong, and the director angle is forced to take the value α. Figure 1 summarizes the setup and notation.

The total (dimensionless) free energy for the system is given by

$$J = \int_0^1 \int_0^L W(\theta, \theta_z)\, dxdz + \int_0^L g_0(x)|_{z=0}\, dx + \int_0^L g_1(x)|_{z=1}\, dx,$$

and equilibrium solutions are those functions $\theta(x, z)$ that minimize J. The standard calculus of variations approach, with $\theta(x, z) \mapsto \theta(x, z) + \epsilon\eta(x, z)$ $(0 < \epsilon \ll 1)$ leads to $J \mapsto J[\theta + \epsilon\eta] = J_0 + \epsilon J_1 + \epsilon^2 J_2 + O(\epsilon^3)$, and for θ to be a minimizer of J we require $J_1 = 0$, $J_2 > 0$, for all admissible variations η (the condition on J_2 ensures we have a minimum, rather than a maximum, of the free energy). After Taylor expansion and integration by parts

$$J_1 = \int_0^1 \int_0^L \eta\left(W_\theta - \left(W_{\theta_z}\right)_z - \left(W_{\theta_x}\right)_x\right) dxdz + \int_0^L \eta(g_{0\theta} - W_{\theta_z})|_{z=0}\, dx + \int_0^L \eta(g_{1\theta} + W_{\theta_z})|_{z=1}\, dx - \int_0^1 \eta W_{\theta_x}|_{x=0}\, dz + \int_0^1 \eta W_{\theta_x}|_{x=L}\, dz.$$

The condition that this vanishes for all admissible variations η leads to the usual Euler-Lagrange equation for θ, subject to boundary conditions on $z = 0$, 1:

$$W_\theta - \left(W_{\theta_x}\right)_x - \left(W_{\theta_z}\right)_z = 0, \quad (8)$$
$$(g_{0\theta} - W_{\theta_z})|_{z=0} = 0, \quad (g_{1\theta} + W_{\theta_z})|_{z=1} = 0. \quad (9)$$

The net contribution to J_1 coming from $x = 0$, 1 is easily seen to vanish for the form of W specified by Eq. (3) if periodic boundary conditions on θ are enforced (both θ and θ_x continuous). We note that the second variation J_2 may be easily calculated if required to check stability. However, in practice we find all steady states by solving a diffusive equation arising from a gradient flow model (below), which guarantees that only stable steady states are found.

B. Time-dependent energetics: Gradient flow

As discussed in [2] for the 1D case, if the system is not initially at equilibrium then it will evolve over time towards a steady state described by the above equations. An accurate description of these dynamics requires the full equations of nematodynamics [20, 26], which couple flow to director reorientation. For our explorations of parameter space that follow, however, the full model is extremely computationally intensive and instead we follow several other authors (e.g. Kedney & Leslie [27] and Davidson & Mottram [24]) in assuming that the system evolves in the direction that minimizes its total free energy (a gradient flow). Both bulk and surface components will evolve in this way, and this process leads to

$$\theta_t + W_\theta - \left(W_{\theta_x}\right)_x - \left(W_{\theta_z}\right)_z = 0,$$
$$(\tilde{\nu}\theta_t + g_{0\theta} - W_{\theta_z})|_{z=0} = 0, \quad (\tilde{\nu}\theta_t + g_{1\theta} + W_{\theta_z})|_{z=1} = 0,$$

with the choice of dimensionless time set by

$$t = t^* \frac{K^*}{\tilde{\mu}^* h^{*2}} \tag{10}$$

where $\tilde{\mu}^*$ is the dimensional rotational viscosity of the NLC molecules, typically around 0.1 N s m^{-2}. The parameter $\tilde{\nu}$ is a dimensionless surface viscosity parameter of size $O(1)$ or smaller [24]; in practice simulations are not very sensitive to the exact value chosen for $\tilde{\nu}$ [28] and we set it to unity throughout. With bulk and surface energy densities given by Eqs. (3) and (6), the system becomes

$$\theta_t = \theta_{xx} + \theta_{zz} - \mathcal{D}\sin 2\theta \tag{11}$$
$$\tilde{\nu}\theta_t = \theta_z - \frac{\mathcal{A}_0}{2}\sin 2(\theta - \alpha_0) + \frac{\mathcal{F}}{2}\sin 2\theta \text{ on } z = 0 \tag{12}$$
$$-\tilde{\nu}\theta_t = \theta_z + \frac{\mathcal{A}_1}{2}\sin 2(\theta - \alpha_1) + \frac{\mathcal{F}}{2}\sin 2\theta \text{ on } z = 1 \tag{13}$$

with $\mathcal{D}$ (dimensionless dielectric coefficient), $\mathcal{F}$ (dimensionless field strength), $\mathcal{A}_{\{0,1\}}$ (dimensionless surface energy) and $\alpha_{\{0,1\}}$ (anchoring angles) given by Eqs. (4), (6) and (7). An initial condition $\theta(x, z, 0)$ closes the model. When θ is independent of time, Eqs. (11)–(13) are exactly the steady-state model, specified by Eqs. (8), (9). We will investigate the multistability and switching properties of Eqs. (11)–(13) as the anchoring perturbation parameters δ, L, ϕ are varied. Before doing so, we first summarize the results of [2] for the analogous 1D model.

C. Summary of results of the 1D model

In the investigation of the 1D model in which anchoring conditions (and hence solutions) are independent of x, it was found that at sufficiently weak anchoring strengths, bistability is possible, with two-way switching between the stable states, effected by transient application of a moderate electric field across the bounding plates. The "switching protocol" adopted when attempting to switch between the stable steady states is as follows: a uniform electric field is applied at a fixed strength (characterized by a fixed value of $|\mathcal{F}|$ with both field directions considered) for t_1 dimensionless time units, and then decreased linearly to zero over a further $t_1/4$ dimensionless time units. For the subset of investigations relevant to the present paper, the field strength was fixed at $|\mathcal{F}| = 5$, while t_1 was fixed at 20 (corresponding to a total dimensional switching time of about 150 ms).

The 1D model was optimized in the parameter space defined by parameters that may be varied in experiments – anchoring strengths and anchoring angles at the two surfaces. The optimization was carried out according to several criteria, principally: (i) maximize the anchoring strengths allowing two-way switching (to maximize robustness); (ii) maximize the optical contrast between the two stable states. If specific weights are assigned to each of the criteria, an "optimal" configuration can be found, and examples of this optimization are given in [2]. The optimization in that paper was carried out in stages, the first stage being an optimization to maximize surface energies (i) and contrast (ii), for the case in which the anchoring angle $\alpha_1^{(0)}$ at the upper surface is related to that at the lower surface, $\alpha_0^{(0)}$, by

$$\alpha_1^{(0)} = \alpha_0^{(0)} - \pi/2. \tag{14}$$

Following this stage the anchoring angle $\alpha_1^{(0)}$ is allowed to vary independently, and then further desirable criteria are introduced into the optimization.

In the final optimal states achieved in the subsequent trials, the anchoring angle $\alpha_1^{(0)}$ is quite close to $\alpha_0^{(0)} - \pi/2$. Therefore, when using this 1D model as the basis for the 2D geometry considered in the present work, we enforce the restriction given by Eq. (14), giving a smaller parameter space to consider. We also use the same "switching protocol" outlined above when testing for switching between the stable states, applying a field of dimensionless strength $|\mathcal{F}| = 5$ for a fixed time interval before decreasing the field linearly to zero. With these restrictions, the entire region of $(\mathcal{A}_0, \mathcal{A}_1, \alpha_0^{(0)})$-space within which bistability with two-way switching is achieved in the 1D model may be mapped out with reasonable computational effort. Figure 2 shows this region. For triplets $(\mathcal{A}_0, \mathcal{A}_1, \alpha_0^{(0)})$ outside this region, no two-way switching is found in the 1D model. Note in particular the existence of definitive upper bounds on the anchoring strengths $\mathcal{A}_0$, $\mathcal{A}_1$, at which the two-way switching is obtained. We also note that, where switching is achieved, in either direction, the sign of the electric field is always the same: $\mathcal{F} = -5$.

III. THE 2D MODEL INVESTIGATIONS

We investigate the effect of adding 2D boundary perturbations of the form (7) to the 1D model. This is motivated by several considerations: (i) it is likely that introducing spatial variation in the boundary will allow the region where two-way switching occurs to be extended; (ii) the 2D system is mathematically more complex and will likely lead to bifurcations to new steady states and

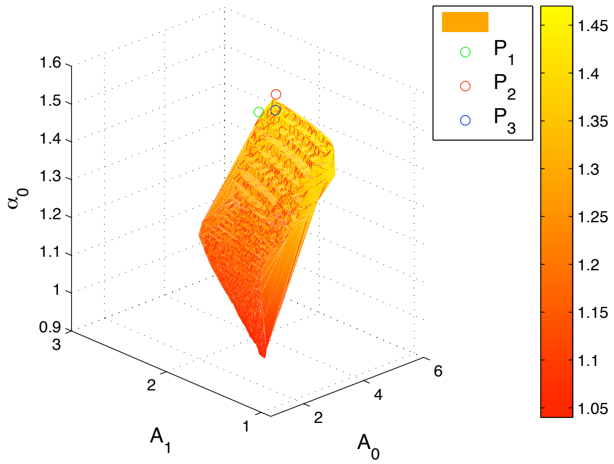

FIG. 2: The 3D-region of $(\mathcal{A}_0, \mathcal{A}_1, \alpha_0^{(0)})$ parameter space within which two-way switching is achieved for the 1D model, showing the particular points P_1, P_2, P_3 used in our investigations of §III. All points lying within the solid shaded region give two-way switching under the given switching protocol. The grayscale (color online) corresponds to the value of the anchoring angle at $z = 0$.

the possible disappearance of old ones; and (iii) in any real device boundary variations are inevitable (even if due only to edge effects) and a 2D study will shed some light on the robustness of the 1D results.

We perturb the 1D model by replacing the constant anchoring angles $\alpha_0^{(0)}$, $\alpha_1^{(0)}$ at the boundaries by sinusoidally-varying angles given by Eq. (7) (with $\alpha_1^{(0)} = \alpha_0^{(0)} - \pi/2$). As noted, though such periodic perturbations are not the most general that could be considered, they do allow for a manageable parametric study to be carried out, and we expect the results to be representative of the more general case. We may view such a perturbation as due either to surface treatment, which alters the surface chemistry and causes the anchoring angle to vary; or as an approximation to the changes in anchoring caused by topographical variation in the bounding surfaces (as in the ZBD or PABD devices [3, 18]). One motivation for allowing such variations is to increase the size of the region where useful two-way switching is possible (relative to that for the 1D model), and a key consideration for robustness of a device to shocks is increasing the allowable anchoring strengths at which the device will work. Hence, we first consider how this might be achieved.

We choose points $(\mathcal{A}_0, \mathcal{A}_1, \alpha_0^{(0)})$ in our parameter space that are *outside* the two-way switching region illustrated in Fig. 2, but close to its boundary. In particular, we increase the surface energies beyond the confines of the 1D switching region. For such points two-way switching is not achievable within the 1D framework; but in 2D it may be possible. We choose three such points to investigate, all in the region of parameter space close to the highest allowable surface energies: points $P_1 = (5.41, 2.45, 1.40)$, $P_2 = (5.50, 2.30, 1.46)$ and $P_3 = (4.85, 2.10, 1.46)$. Other points (including some that are far from the 1D optimum) were investigated, but did not yield significantly different results from those for these three points.

For each chosen point we perturb the anchoring boundary conditions in several ways. (i) Perturb the anchoring only at the lower boundary. This involves setting $\delta_1 = 0$ in Eq. (7) and, with no loss of generality, $\phi_0 = 0$, leaving just two perturbation parameters δ and L. (ii) Perturb the anchoring at both boundaries, with the same amplitude $\delta_1 = \delta_0 = \delta$, and with no phase difference between the boundaries: $\phi_0 = 0$, leaving just two perturbation parameters δ and L. (iii) Perturb the anchoring at both boundaries, with the same amplitude $\delta_1 = \delta_0 = \delta$, and with variable phase difference between the boundaries: $\phi_0 = \phi \in [0, \pi/2]$, but fixing the domain length L. This again leaves just two perturbation parameters, δ and ϕ.

We describe the outcome of these investigations below. In all cases we use numerical continuation to generate our basic stable states. We start from the 1D problem, where the two stable steady states, which we label $\boldsymbol{n}_1$ and $\boldsymbol{n}_2$, are known analytically [2]. We apply a small perturbation, $\delta = 0.1$, using each 1D steady state as an initial condition in Eqs. (11)–(13) (at zero field, $\mathcal{D} = \mathcal{F} = 0$). We solve these equations using a standard ADI scheme, and look for steady-state solutions, which are in practice found by evolving Eqs. (11)–(13) until the results do not change further (typically it is enough to simulate until $t = 30$ (dimensionless time units) to ensure that true steady-state solutions are found). Then, we use these newly found steady-state solutions as initial conditions for the more strongly perturbed case, with $\delta = 0.2$, and so on. If at any stage a new steady state appears, backward continuation in δ is used to locate its first appearance. We then subject all solutions found to our switching protocol (apply a transient electric field, as for the 1D case described in §II C above). It is possible that this produces new steady states. If this happens, these states are also tracked using continuation in δ, as described above.

To illustrate further the coexistence of the multiple steady states and the transitions between them, we also construct bifurcation diagrams in several cases, by plotting a norm of the (stable) steady states versus δ:

$$\mathrm{norm}(\boldsymbol{n}) := \sqrt{\sum_{i,j=1}^{M,N} \left(\frac{\theta_{i,j}(\mathrm{mod}.\pi)^2)}{MN} \right)}, \qquad (15)$$

where $\theta_{i,j}$ is the discretization of the director angle θ at grid point (i, j), and M, N are the total number of mesh grid points in each direction. The different steady states have different norms, hence the solution branches are distinct when plotted in this way and bifurcations are evident. Since (as described above) all steady states are found by time-evolving the dynamic system until no further change is seen, this method of constructing the bifurcation diagram can produce only the stable solution branches. No unstable steady solutions are found by our methods.

IV. RESULTS

We summarize our results for each type of boundary perturbation, and for each of the three chosen "test points" in parameter space, below. The system exhibits rich behavior, with as many as four distinct steady states found in certain parameter regimes. We label these four steady states $\boldsymbol{n}_1$, $\boldsymbol{n}_2$, $\boldsymbol{n}_3$, $\boldsymbol{n}_4$. In accordance with our continuation methods, $\boldsymbol{n}_1$ and $\boldsymbol{n}_2$ are always the continuations of the 1D steady states found in the unperturbed problem (consistent with the results of [2]), while $\boldsymbol{n}_3$ and $\boldsymbol{n}_4$ are new states that only exist with perturbed anchoring. The results on switching are presented symbolically to denote the outcome at each point in parameter space, with reference to the global legend presented in Fig. 3. Each symbol in that legend records which steady states exist (listed within braces $\{\cdot\}$), and what switching is found between those states (denoted by directional arrows as described in the caption). An example of three coexisting steady states is shown in Fig. 4.

We note that exploring the complete 3D parameter space considered would be computationally very demanding. The discussion that follows is limited to illustrating just some features of the results that may be expected.

A. Equal-amplitude perturbations to anchoring angles at both boundaries with zero phase difference

Here we consider the domain with anchoring angles α_0, α_1 at lower and upper boundaries given by

$$\begin{aligned}\alpha_0 &= \alpha_0^{(0)} + \delta\cos(2\pi x/L),\\ \alpha_1 &= \alpha_0^{(0)} - \pi/2 + \delta\cos(2\pi x/L),\end{aligned} \tag{16}$$

as the perturbation amplitude δ and domain length L vary.

1. *Point* P_1, $(\mathcal{A}_0, \mathcal{A}_1, \alpha_0^{(0)}) = (5.41, 2.45, 1.40)$

Figure 5 shows the results of the switching investigation when the 1D case represented by point P_1 in $(\mathcal{A}_0, \mathcal{A}_1, \alpha^{(0)})$-space is perturbed at both boundaries, with no phase difference, as in Eq. (16). We see that for sufficiently small perturbation amplitude δ the continuations of the two 1D stable steady states exist and there is still no two-way switching between them. This is to be anticipated, since the point P_1 lies outside the switching region for the 1D problem. As δ increases however, more complex behavior emerges.

For sufficiently small values of L, once δ passes a first threshold value, a window of two-way switching $\boldsymbol{n}_1 \leftrightarrow \boldsymbol{n}_2$ is observed. This is already a significant finding, since it shows that two-way switching is possible in the 2D geometry even if it does not occur for the 1D case. This window disappears when δ passes a second threshold value. Both threshold values decrease as L increases. When δ is increased further still, a new steady state $\boldsymbol{n}_3$ is observed. As an illustration, Fig. 4 shows $\boldsymbol{n}_1$, $\boldsymbol{n}_2$, $\boldsymbol{n}_3$ as vector plots in (x, z)-space over a single wavelength, for $(L, \delta) = (4, 0.7)$.

For small values of L, $\boldsymbol{n}_3$ appears to arise from a pitchfork bifurcation of $\boldsymbol{n}_1$ and $\boldsymbol{n}_2$, as shown in Fig. 6. This figure shows a bifurcation diagram, constructed by plotting a norm of the (stable) steady states versus δ (see Eq.(15)), Figure 6 shows bifurcation diagrams for the cases $L = 0.5$ and $L = 4$: the case $L = 0.5$ clearly indicates the pitchfork bifurcation. For this value of L the stable steady state $\boldsymbol{n}_3$ never coexists with stable steady states $\boldsymbol{n}_1$ and $\boldsymbol{n}_2$, but replaces them at large δ. As described in §III, these bifurcation diagrams show only the stable solution branches; unstable steady solutions are not found by our methods.

Figure 5 shows that for larger values of L, $L \gtrsim 2$, the two-way switching between $\boldsymbol{n}_1$ and $\boldsymbol{n}_2$ is suppressed. The stable steady state $\boldsymbol{n}_3$ appears sooner, at smaller values of δ, and now coexists with $\boldsymbol{n}_1$ and $\boldsymbol{n}_2$. For $L = 3$, although there is no two-way switching $\boldsymbol{n}_1 \leftrightarrow \boldsymbol{n}_2$, we do find two-way switching between $\boldsymbol{n}_2$ and $\boldsymbol{n}_3$ (for $\delta = 0.6, 0.7$, and presumably also in some surrounding neighborhood of (L, δ)-space), and for $\delta = 0.5$ it is particularly interesting to observe *cyclic* switching involving all three steady states: we see the switching sequence $\boldsymbol{n}_1 \to \boldsymbol{n}_3 \to \boldsymbol{n}_2 \to \boldsymbol{n}_1$. We expect that this cyclic switching occurs in some small surrounding neighborhood of (L, δ)-space.

For $L = 6$ (the largest value of L considered) the steady state $\boldsymbol{n}_3$ appears even for the smallest value of δ used, $\delta = 0.1$. More generally, though more steady states exist with (one would imagine) greater potential for switchability for larger L, no two-way switching is found for $L > 3$. Another consequence of longer domains (larger L) is an increased degree of solution complexity, as is apparent from the bifurcation diagram shown in Fig. 6(b).

The steady state $\boldsymbol{n}_3$, once formed, appears rather robust under the conditions investigated here: other than the switching noted above for $L = 3$, and $\boldsymbol{n}_3 \to \boldsymbol{n}_2$ switching at small δ for $L = 6$, no switching was found from this state to any other. Far more switching is found from the steady states $\boldsymbol{n}_1$ and $\boldsymbol{n}_2$ to other states.

2. *Point* P_2, $(\mathcal{A}_0, \mathcal{A}_1, \alpha_0^{(0)}) = (5.50, 2.30, 1.46)$

Figure 7 shows results when the 1D case represented by point P_2 in $(\mathcal{A}_0, \mathcal{A}_1, \alpha^{(0)})$ is perturbed at both boundaries, with no phase difference, as in Eq. (16). For very short domains, no two-way switching is found, at any perturbation amplitude. Only the two steady states $\boldsymbol{n}_1$ and $\boldsymbol{n}_2$ exist until $\delta = 0.9$, when the third steady state $\boldsymbol{n}_3$ appears. This state replaces both $\boldsymbol{n}_1$ and $\boldsymbol{n}_2$; see also the bifurcation plot in Fig. 8(a). As the length L is increased slightly (as with the point P_1) a window of two-way switching opens for a range of δ-values. Again, at higher δ the third steady state $\boldsymbol{n}_3$ appears, and the

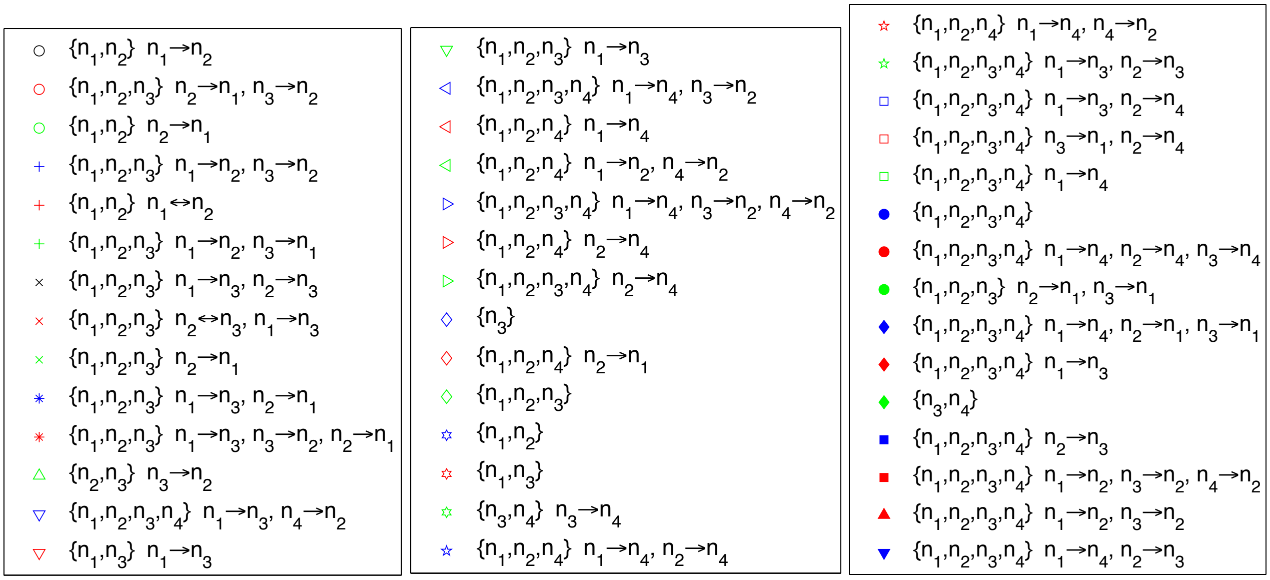

FIG. 3: (Color online.) Explanation of symbols used in the switching results that follow below. The notation within braces denotes which steady states exist at a given point in parameter space. The statement $\mathrm{n_i} \to \mathrm{n_j}$ denotes that switching occurs from state $\boldsymbol{n}_i$ to $\boldsymbol{n}_j$; and $\mathrm{n_i} \leftrightarrow \mathrm{n_j}$ denotes that two-way switching occurs between states $\boldsymbol{n}_i$ and $\boldsymbol{n}_j$.

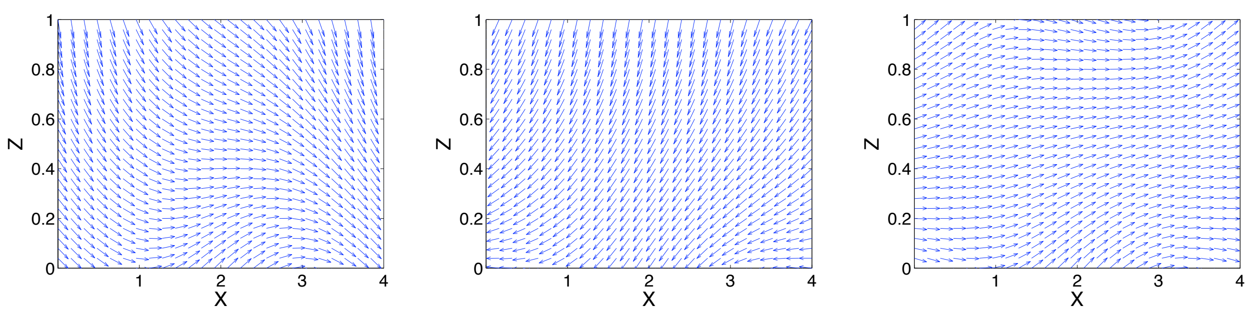

FIG. 4: The three steady states (a-c) $\boldsymbol{n}_1$, $\boldsymbol{n}_2$, $\boldsymbol{n}_3$, corresponding to the point $(L, \delta) = (4, 0.7)$ in Fig. 5.

δ-value at which $\boldsymbol{n}_3$ appears decreases as L increases. At $L = 2$ yet another steady state $\boldsymbol{n}_4$ appears at large δ: at this L-value as δ increases we have just two steady states for $0 \le \delta \le 0.5$, with two-way switching for $\delta = 0.3, 0.4$; for $\delta = 0.6, 0.7$ three steady states $\boldsymbol{n}_1$, $\boldsymbol{n}_2$, $\boldsymbol{n}_3$ coexist; for $\delta = 0.8$ just $\boldsymbol{n}_3$ exists; and for $\delta = 0.9$ the new steady state $\boldsymbol{n}_4$ comes into existence, coexisting with $\boldsymbol{n}_3$. No further two-way switching is found, however. For larger values $L > 3$, though the solution space becomes much richer and more complex, no two-way switching is found between any pair of stable states, even though for some parameter ranges all four steady states can coexist (see the bifurcation diagram for $L = 4$ in Fig. 8(b) where the four states coexist for a wide range of δ values). The steady state $\boldsymbol{n}_4$ appears to be particularly stable here, since it does not switch to any other state.

The trend of two-way switching for smaller domains, and of increased solution complexity for longer domains, is as seen for the point P_1 described above. Increased complexity could be loosely explained based on the increased ability of the director orientation to find additional configurations; however, we do not have a good explanation for the lack of two- way switching for these large domains.

Examples of the four steady states that can coexist are shown in Fig. 9.

3. *Point* P_3, $(\mathcal{A}_0, \mathcal{A}_1, \alpha_0^{(0)}) = (4.85, 2.10, 1.46)$

Figure 10 shows results when the 1D case represented by point P_3 in $(\mathcal{A}_0, \mathcal{A}_1, \alpha^{(0)})$-space is perturbed at both boundaries, with no phase difference, as in Eq. (16). This case differs from the previous two: the region of two-way switching has shrunk considerably, to some small neighborhood of the point $(L, \delta) = (1, 0.5)$. As with the two other points though, the solution space complexity increases markedly as L increases: for $L \ge 1$ we find three solutions can coexist ($\boldsymbol{n}_1$, $\boldsymbol{n}_2$ and $\boldsymbol{n}_3$), while for $L \ge 4$ we again find four solutions that can coexist for a wide

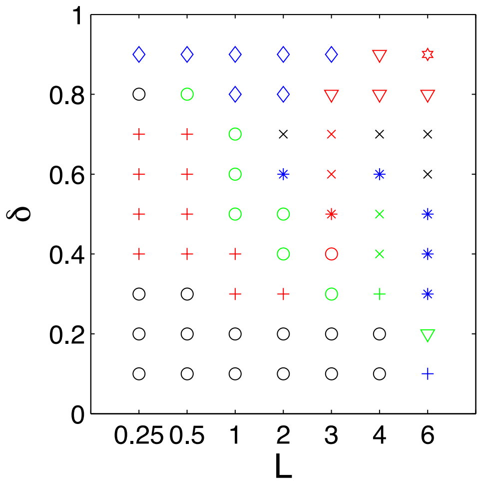

FIG. 5: Switching results when perturbing the 1D case represented by point P_1, $(\mathcal{A}_0, \mathcal{A}_1, \alpha_0^{(0)}) = (5.41, 2.45, 1.40)$, according to Eq. (16). Symbols are defined in the global legend of Fig. 3.

range of δ-values. This increase in solution complexity may again be illustrated by bifurcation diagrams as the bifurcation parameter δ is increased: Fig. 11 shows the bifurcation diagrams for $L = 0.5$ and $L = 4$. As usual, the shorter domain length leads to a simple pitchfork bifurcation.

B. Equal-amplitude perturbations to anchoring angles at both boundaries with phase difference

In this section we consider the case with anchoring angles α_0, α_1 at lower and upper boundaries given by

$$\alpha_0 = \alpha_0^{(0)} + \delta\cos(2\pi x/L + \phi),$$
$$\alpha_1 = \alpha_0^{(0)} - \pi/2 + \delta\cos(2\pi x/L), \tag{17}$$

as the perturbation amplitude δ and phase-shift ϕ vary. For each point in parameter space considered, motivated by the underlying application (which requires two-way switching for utility) we fix the domain length L at the "most promising" value indicated by the results of §IV A.

1. *Point* P_1, $(\mathcal{A}_0, \mathcal{A}_1, \alpha_0^{(0)}) = (5.41, 2.45, 1.40)$

For this point, the (equal) best domain length in terms of achieving the largest window of two-way switching, as indicated by the results of §IV A, Fig. 5, is $L = 0.5$. We therefore consider the influence of introducing a phase difference, ϕ, into the anchoring variations on both boundaries, as indicated in Eq. (17) above, with L fixed at this value.

Figure 12 shows the results as the phase difference in boundary conditions, Eq. (17), is increased from $\phi = 0$ to $\phi = \pi$. Note that for this and the subsequent points considered, the results for $\pi \le \phi \le 2\pi$ may be obtained by reflecting Fig. 5 about $\phi = \pi$. Curiously, the results are almost independent of the phase difference, a sizeable window of two-way switching persisting for all values of ϕ tested. No pattern of increasing solution complexity emerges here: the third steady state $\boldsymbol{n}_3$ is always observed only for large δ, and no fourth steady state is found.

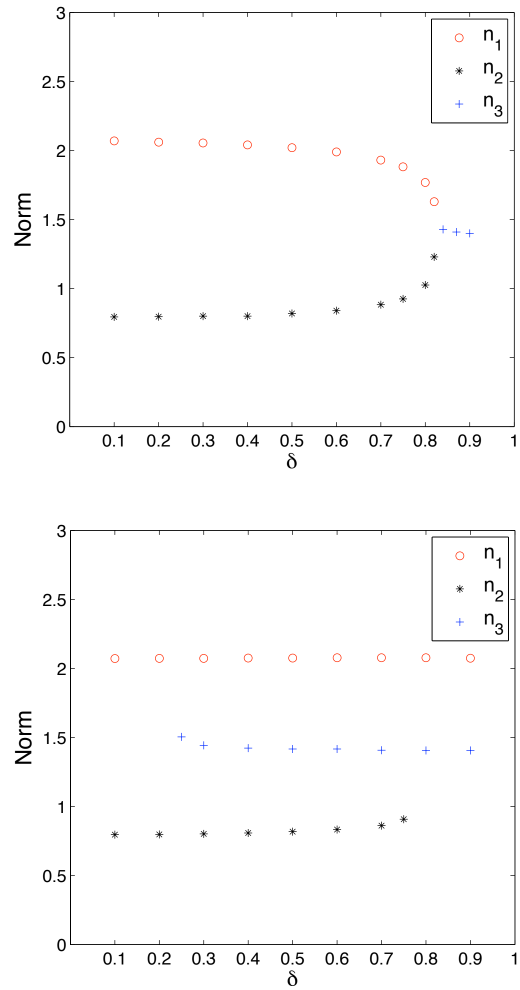

(a)

(b)

FIG. 6: Bifurcation diagrams representing stable steady states obtained when perturbing the 1D case represented by point P_1, $(\mathcal{A}_0, \mathcal{A}_1, \alpha_0^{(0)}) = (5.41, 2.45, 1.40)$, for the cases $L = 0.5$ (a) and $L = 4$ (b).

2. *Point* P_2, $(\mathcal{A}_0, \mathcal{A}_1, \alpha_0^{(0)}) = (5.50, 2.30, 1.46)$

For this point, the best domain length in terms of achieving the largest window of two-way switching, as indicated by the results of §IV A, Fig. 7, is again $L = 0.5$. Figure 13 shows the results as the phase difference in Eq. (17) is increased from $\phi = 0$ to $\phi = \pi$. In this case the

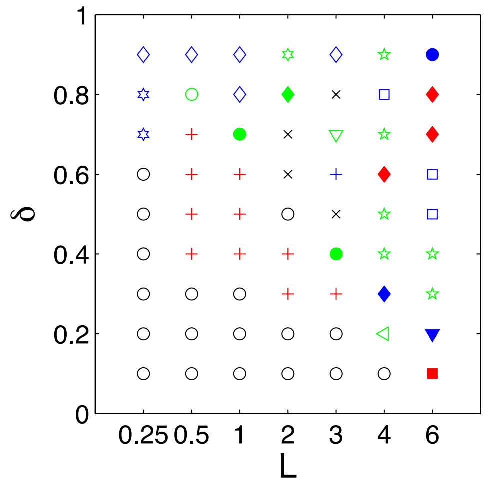

FIG. 7: Switching results when perturbing the 1D case represented by point P_2, $(\mathcal{A}_0, \mathcal{A}_1, \alpha_0^{(0)}) = (5.50, 2.30, 1.46)$, according to Eq. (16). Symbols are defined in the global legend of Fig. 3.

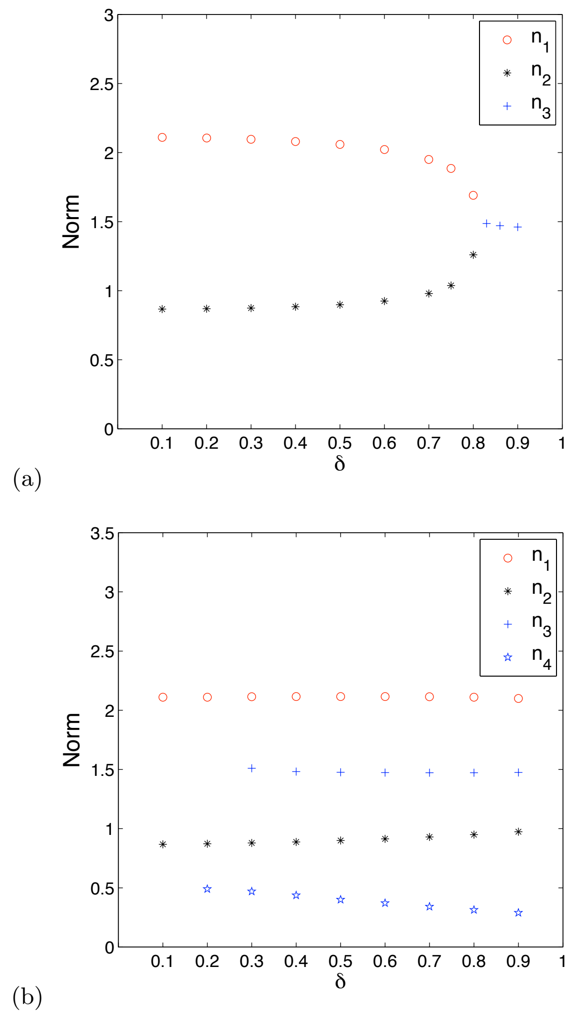

FIG. 8: Bifurcation diagrams representing stable steady states obtained when perturbing the 1D case represented by point P_2, $(\mathcal{A}_0, \mathcal{A}_1, \alpha_0^{(0)}) = (5.50, 2.30, 1.46)$, for the cases $L = 0.5$ (a) and $L = 4$ (b).

window of two-way switching shrinks as ϕ is increased, and disappears. Otherwise, the behavior is similar to that observed for point P_1 above: there is no evidence of increasing solution complexity as ϕ is varied; $\boldsymbol{n}_3$ is found only at large δ; and no fourth steady state is ever found.

3. Point P_3, $(\mathcal{A}_0, \mathcal{A}_1, \alpha_0^{(0)}) = (4.85, 2.10, 1.46)$

For this point, two-way switching was observed in the results of §IV A only for the domain length $L = 1$ (see Fig. 10), hence we fix $L = 1$ here.

Figure 14 shows the results as the phase difference in Eq. (17) is increased from $\phi = 0$ to $\phi = \pi$. As with point P_1, little variation with ϕ is observed. The small window of two-way switching persists until $\phi = \pi/2$, after which it vanishes. The steady state $\boldsymbol{n}_3$ appears at the same δ value for all phase shifts ϕ ($\delta = 0.7$), in coexistence with $\boldsymbol{n}_1$ and $\boldsymbol{n}_2$ for $0 \leq \phi \leq \pi/2$, and in coexistence with $\boldsymbol{n}_2$ only for $\phi > \pi/2$ (so the bifurcation structure changes slightly as ϕ is increased).

To conclude, though we carried out only limited tests, it does not appear that introducing phase difference into the boundary conditions leads to increased two-way switching.

C. Perturbation to anchoring angle at one boundary only

In this section we investigate the effects of anchoring variations at one bounding surface only (we choose the lower surface). The anchoring angles imposed when solving Eqs. (11)–(13) are

$$\alpha_0 = \alpha_0^{(0)} + \delta \cos(2\pi x/L), \quad \alpha_1 = \alpha_0^{(0)} - \pi/2. \qquad (18)$$

1. Point P_1, $(\mathcal{A}_0, \mathcal{A}_1, \alpha_0^{(0)}) = (5.41, 2.45, 1.40)$

Figure 15 shows that, in line with our earlier results, increasing the domain length, L, is associated with increasing solution complexity; though the switching obtained is less complex than in §IV A where both boundaries are perturbed. No two-way switching is ever found, nor any switching cycles, therefore in this instance at least, perturbing just the one boundary does not appear to be advantageous.

2. Point P_2, $(\mathcal{A}_0, \mathcal{A}_1, \alpha_0^{(0)}) = (5.50, 2.30, 1.46)$

Figure 16 shows the results of a perturbation represented by Eq. (18) to the anchoring conditions on the lower boundary only, the unperturbed case being represented by point P_2 in the 1D problem. The same general

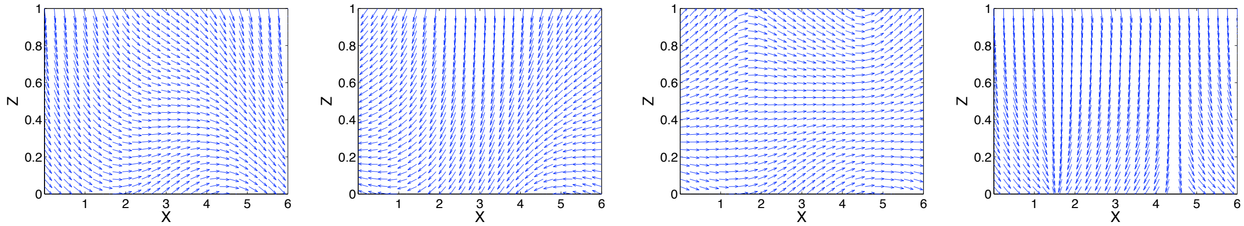

FIG. 9: The four steady states (a-d) $\boldsymbol{n}_1$, $\boldsymbol{n}_2$, $\boldsymbol{n}_3$, $\boldsymbol{n}_4$, corresponding to the point $(L, \delta) = (6, 0.6)$ in Fig. 7.

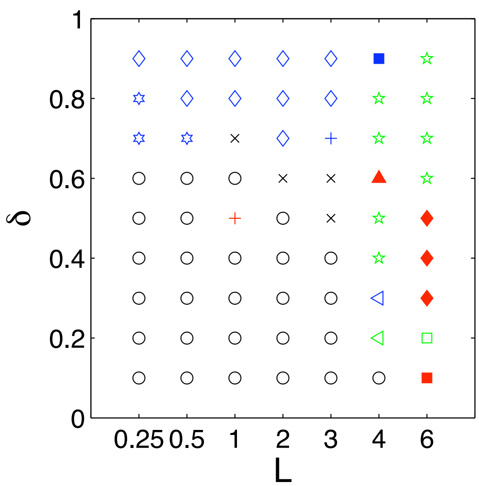

FIG. 10: Switching results when perturbing the 1D case represented by point P_3, $(\mathcal{A}_0, \mathcal{A}_1, \alpha_0^{(0)}) = (4.85, 2.10, 1.46)$, according to Eq. (16). Symbols are defined in the global legend of Fig. 3.

observations as for point P_1 above hold: again, increasing the domain length, L, is clearly associated with increasing solution complexity, but behavior is overall less complex than in §IV A where both boundaries are perturbed. No two-way switching or switching cycles are found for any (L, δ)-values tested, therefore for P_2 this type of boundary perturbation also does not lead to desired two-way switching.

3. *Point* P_3, $(\mathcal{A}_0, \mathcal{A}_1, \alpha_0^{(0)}) = (4.85, 2.10, 1.46)$

Figure 17 shows the results for point P_3 in the 1D problem. This case behaves similarly to points P_1 and P_2 above, with increasing L leading to increased complexity, but with no useful two-way or cyclic switching found.

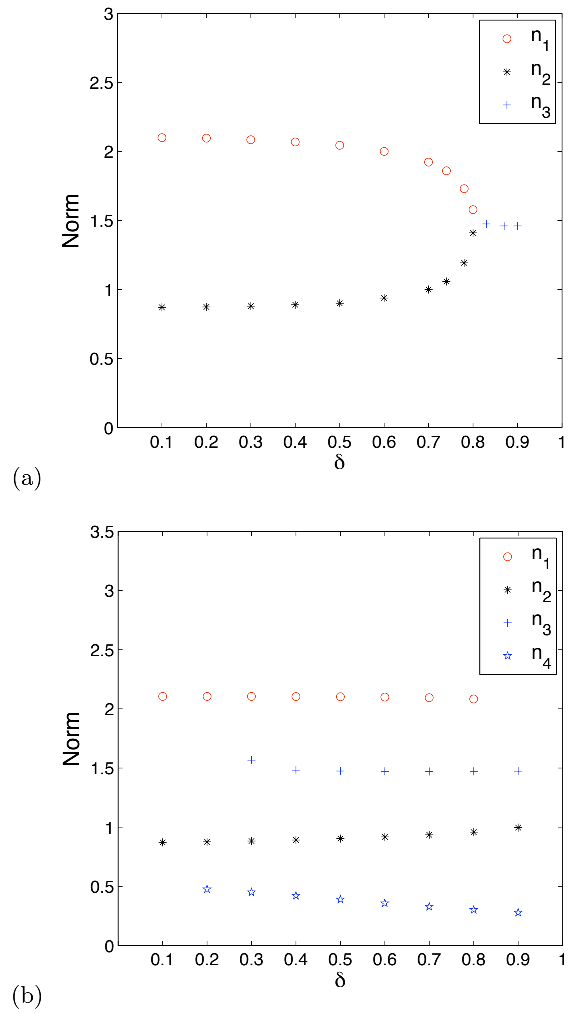

FIG. 11: Bifurcation diagrams representing stable steady states obtained when perturbing the 1D case represented by point P_3, $(\mathcal{A}_0, \mathcal{A}_1, \alpha_0^{(0)}) = (4.85, 2.10, 1.46)$, for the cases $L = 0.5$ (a) and $L = 4$ (b).

V. DISCUSSION AND CONCLUSIONS

We have taken a basic but promising 1D model for a bistable LCD device [2], and investigated how it behaves under a specific class of spatial perturbations to the anchoring boundary conditions (sinusoidal perturbations to the anchoring angles at the flat bounding surfaces). While more general periodic boundary perturbations could be considered, we restrict attention to those of the form (7), because they afford a manageable parameter space to study, and because we believe the results will be representative of the more general case. Such pertur-

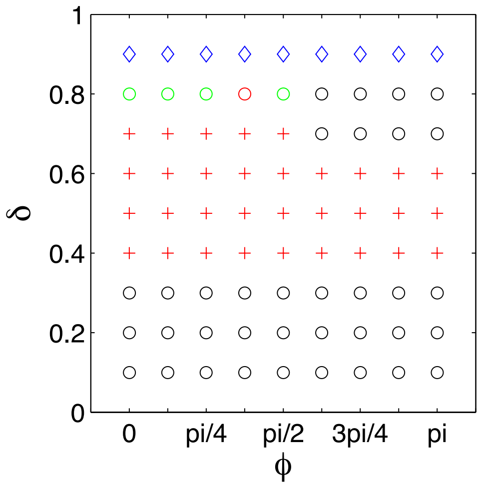

FIG. 12: Switching results when perturbing the 1D case represented by point P_1, $(\mathcal{A}_0, \mathcal{A}_1, \alpha_0^{(0)}) = (5.41, 2.45, 1.40)$, according to Eq. (17). The domain length is fixed at $L = 0.5$. Symbols are defined in the global legend of Fig. 3.

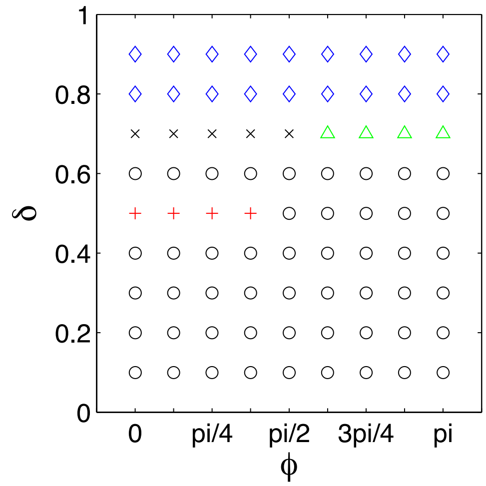

FIG. 14: Switching results when perturbing the 1D case represented by point P_3, $(\mathcal{A}_0, \mathcal{A}_1, \alpha_0^{(0)}) = (4.85, 2.10, 1.46)$, according to Eq. (17). The domain length is fixed at $L = 1$. Symbols are defined in the global legend of Fig. 3.

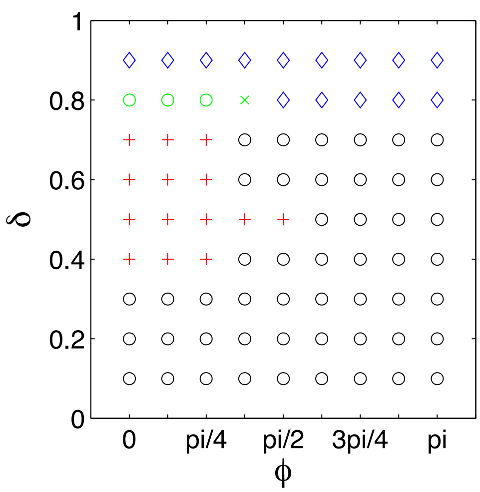

FIG. 13: Switching results when perturbing the 1D case represented by point P_2, $(\mathcal{A}_0, \mathcal{A}_1, \alpha_0^{(0)}) = (5.50, 2.30, 1.46)$, according to Eq. (17). The domain length is fixed at $L = 0.5$. Symbols are defined in the global legend of Fig. 3.

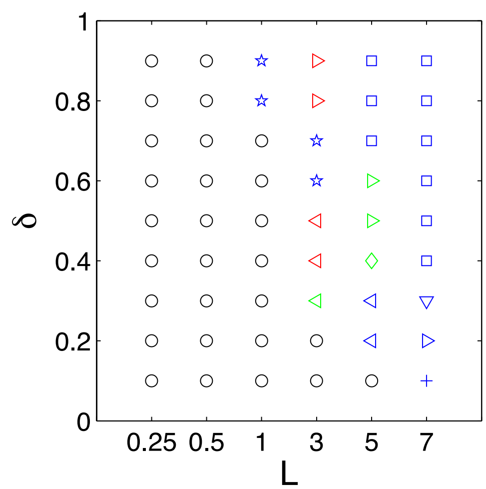

FIG. 15: Switching results when perturbing the 1D case represented by point P_1, $(\mathcal{A}_0, \mathcal{A}_1, \alpha_0^{(0)}) = (5.41, 2.45, 1.40)$, according to Eq. (18). The lower boundary only is perturbed, and δ and L vary. Symbols are defined in the global legend of Fig. 3.

bations to the anchoring angles could be due to periodic chemical gradients imposed at the surfaces, or may be thought of as approximating a device with periodic topographical variations. The study of such variations is important for two reasons: firstly, it may provide useful indications of how to tune boundaries to create a workable bistable device of this kind, which improves on the simpler 1D model proposed in [2]; and secondly, it affords insight into the robustness of the underlying 1D device to engineering imperfections.

Our results are presented for a few chosen sample points in the space of surface energies $\mathcal{A}_0$, $\mathcal{A}_1$, at the upper and lower bounding surfaces respectively, and unperturbed anchoring angle $\alpha_0^{(0)}$ at the lower bounding surface, as outlined in §II C and §III. The motivation for choosing these test points was that they lie nearby the most promising region of parameter space for the 1D model, but when unperturbed, do not permit two-way switching [2]. Perturbing a 1D device based on these points therefore gives some insight into whether 2D effects can lead to improvements over the 1D results. The unperturbed anchoring angle at the upper bounding surface, $\alpha_1^{(0)}$, is fixed by Eq. (14). Both anchoring angles are systematically perturbed according to three different protocols, described in §IV A (in-phase,

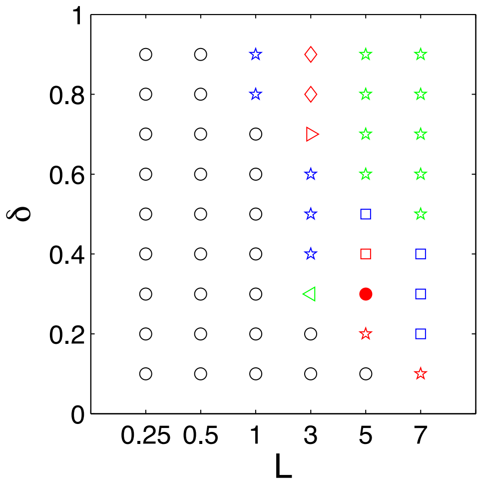

FIG. 16: Switching results when perturbing the 1D case represented by point P_2, $(\mathcal{A}_0, \mathcal{A}_1, \alpha_0^{(0)}) = (5.50, 2.30, 1.46)$, according to Eq. (18). The lower boundary only is perturbed, and δ and L vary. Symbols are defined in the global legend of Fig. 3.

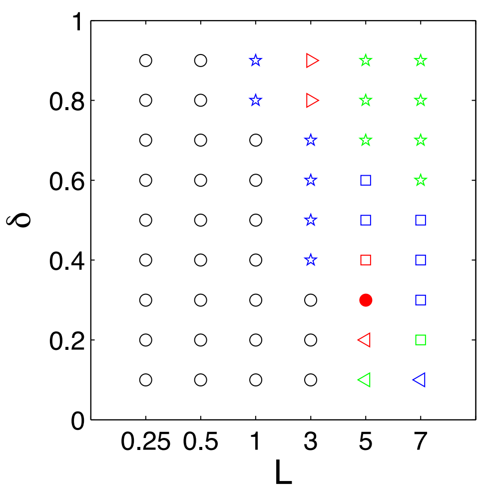

FIG. 17: Switching results when perturbing the 1D case represented by point P_3, $(\mathcal{A}_0, \mathcal{A}_1, \alpha_0^{(0)}) = (4.85, 2.10, 1.46)$, according to Eq. (18). The lower boundary only is perturbed, and δ and L vary. Symbols are defined in the global legend of Fig. 3.

variable-amplitude, variable wavelength perturbations to both angles), §IV B (variable phase, variable amplitude, fixed wavelength perturbations to both angles) and §IV C (variable amplitude, variable wavelength perturbations to one angle only). Where both boundaries are perturbed, the perturbation amplitude, δ, is the same at each boundary; where only the lower boundary is perturbed, the phase difference, ϕ, is zero by default. Since only two of the three variables δ, L (domain length) and ϕ are perturbed in any set of experiments, our results on the steady states found and switching between them can be represented graphically by 2D parametric plots.

For all cases studied the perturbations lead to surprisingly rich behavior when compared with the 1D case. As we would expect, for sufficiently small δ, the results are close to those found in 1D: only two stable steady states, with no two-way switching under transient application of an electric field. However, for a given L we find a threshold value δ^* at which a bifurcation occurs and new steady states are found. This threshold value δ^* decreases as L increases. Depending on the value of L, the new steady state(s) may either replace the continuations of the original steady states $\boldsymbol{n}_1$ and $\boldsymbol{n}_2$ (a simple pitchfork bifurcation; Figs. 6(a), 8(a), 11(a)), or else coexist with them (a saddle-node bifurcation; Figs. 6(b), 8(b), 11(b)). Though a full bifurcation study was not performed, our results indicate that short domains (small L) lead to a pitchfork bifurcation in which bistability yields to monostability, while long domains give a more complex bifurcation structure with folds, in which multiple distinct steady states can coexist (in the cases we considered, up to four states were found simultaneously). The bifurcation to tri- and tetrastability can occur at very small δ^* for the largest L's considered. Somewhat surprisingly, introducing a phase difference between perturbations at the two boundaries does not have a significant effect on the results obtained, at least for the domains considered.

On the one hand, our results indicate that long-wavelength perturbations of even very small amplitude may introduce significant complexity, in particular multiple stable steady states, but with a lack of reversible switching between them. While interesting from a scientific point of view, this finding also has a practical consequence, since it suggests that such perturbations are not useful if a reliable bistable device with two-way switching is desired. This finding also suggests that an unperturbed device, of the kind discussed in [2], may be unstable if the domain length is large, with possible multistability and undesired complexity.

On the other hand, we do find a sizeable set of boundary perturbations for which two-way switching is found between states $\boldsymbol{n}_1$ and $\boldsymbol{n}_2$, for parameters for which two-way switching is not possible in the unperturbed case. Even more interestingly, we find that two-way switching between the newly-found $\boldsymbol{n}_3$ state and the $\boldsymbol{n}_2$ state, as well as cyclic switching $\boldsymbol{n}_1 \to \boldsymbol{n}_3 \to \boldsymbol{n}_2 \to \boldsymbol{n}_1$, may occur. Therefore, we find significant potential utility of the boundary perturbations, particularly of shorter wavelengths, provided one can make boundary modifications of wavelength comparable to or smaller than the device thickness, and of reasonable amplitude. Presumably the finite-sized amplitude of such perturbations would be sufficient to destroy the undesired sensitivity to long-wavelength, small amplitude perturbations noted above. Though both directions of the electric field are considered when testing for switching ($\mathcal{F} = \pm 5$), the switching is always found for $\mathcal{F} = -5$ (this was also the case for the 1D problem [2]).

We note that our results are also of interest when compared to theoretical simulations of the so-called ZBD (Zenithal Bistable Device) [3]. In that device a 2D model is found to permit bistability and two-way switching via boundary perturbations (geometric, for the ZBD); but one of the two steady states always has a disclination. Our model suggests that a truly 2D bistable switchable device may in fact be possible without any disclinations.

Throughout this study, in our switching investigations it was assumed that the electric field, when applied, is uniform throughout the NLC. In reality of course there is interaction between the field and the NLC, leading to nonuniformities in the field. A preliminary investigation into the size of such deviations from uniformity for the 1D model suggests that, under typical operating conditions, they are small [4]; more details of nonuniform field effects will be published in a forthcoming paper. We have not explored extensively the influence of the strength or duration of the applied electric field but, based on our previous analysis of the one dimensional configuration in [2], we would not expect to see significant influence of these quantities on the presented results (the field is simply the means by which switching is effected: as long as it is sufficiently strong and applied for sufficiently long, which we believe is the case in the present paper, then if switching is theoretically possible it should be observed).

We do not, in this paper, carry out a detailed study of optical contrast between the stable states found, since we are far from producing any kind of optimal device of this kind. We note however that optical contrast ratios were calculated for the 1D solutions of [2] from which our 2D solutions derive, and were found to be generally good. In addition, the bifurcation plots in the present paper, showing the norm of the director field versus perturbation amplitude, provide some crude estimate of the contrast between the steady states.

In this work, we have considered a three dimensional parameter space defined by ($\mathcal{A}_0$, $\mathcal{A}_1$, $\alpha_0^{(0)}$). It is clearly difficult to analyze this large space in detail by the present methods, and we certainly cannot claim that the results found at the considered isolated points cover the whole range of possible behavior. For example, we found that up to four steady states can co-exist in some cases; however even more complex scenarios with a larger number of stable solutions are possible. Despite the limitations of the presented analysis, our results do suggest that improvements from the unperturbed 1D configurations are possible; however, the extent of these improvements may depend on the choice of physical parameters (anchoring strengths and angles). In addition, our results strongly suggest that short wavelength perturbations are more promising if formulation of a bistable switchable device is desired. A more detailed study, beyond the scope of the present paper, is required to determine the true utility of such a device. More points in parameter space should be considered to confirm the generality of our findings for the few points studied here; and for the most promising short-wavelength boundary perturbations, a detailed study of the energy landscape should be made (the energy barriers between stable states should be neither too high to surmount, nor too low for robustness to shocks), and the optical contrast ratios calculated.

Finally, we note that, of course, all of our results here are restricted to two space dimensions, and take no account of three-dimensional effects. The 2D problem for the director field in an NLC is rather special, since $\boldsymbol{n}$ may be described in terms of a single polar angle, θ. If 3D variations are permitted to either device boundary then a second (azimuthal) angle ϕ is required to characterize the director, and a system of coupled PDEs for θ and ϕ (arising from the gradient flow model due to the more complicated free energy describing 3D elastic deformation) must be solved. Even for simple classes of 3D perturbations to the bounding surfaces, and for the simplest case of conical anchoring on ϕ at both surfaces, we might expect the results to be correspondingly richer still than those presented here.

Acknowledgments

This work was supported by the NSF under grants DMS-0908158 and DMS-1211713. LJC also gratefully acknowledges partial support from King Abdullah University of Science and Technology (KAUST) in the form of an OCCAM Visiting Fellowship, funded by Award no. KUK-C1-013-04.

[1] Kosc, T.Z. (2005) Particle display technologies become E-Paper. *Optics & Photonics News*, **16** (2), 18-23.

[2] Cummings, L.J., Cai, C., Kondic, L. (2013) Towards an optimal model for a bistable nematic liquid crystal display device. *J. Eng. Math.* **80** (1), 21-38.

[3] Bryan-Brown, G.P., Brown, C.V., Jones, J.C. (1995) U.S. Patent 6249332 (Zenithal Bistable Device).

[4] Cai, C. (2013) Mathematical models for bistable nematic liquid crystal displays. *Ph.D. Thesis, NJIT.*

[5] Chen, T.-J., Chu, K.-L. (2008) Pretilt angle control for single-cell-gap transflective liquid crystal cells. *Appl. Phys. Lett.* **92** (9), 091102.

[6] Cui, L., Jin, W., Liu, Y., Xie, P., Zhang, R., Zhu, C., Wang, C. (1999) A combined method based on rubbing and UV-irradiation for preparing stable alignment layers with high pretilt angles. *Mol. Cryst. Liq. Cryst.* **333**, 135-144.

[7] Hwang, J.-Y., Lee, S.H., Paek, S.K., Deo, D.-S. (2003) Tilt angle generation for nematic liquid crystal on blended homeotropic polyimide layer containing Trifluoromethyl moieties. *Jpn. J. Appl. Phys.* **42** (1), 1713-1714.

[8] Kim, K.-H., Baek, J.-I., Cheong, B.-H., Choi, H.-Y., Shin, S.T., Kim, J.C., Yoon, T.-H. (2010) Pretilt angle control and multidomain alignment of liquid crystals by using polyimide mixed with liquid crystalline prepolymer. *Appl. Phys. Lett.* **96** (21), 213507.

[9] Komitov, L., Barbero, G., Dahl, I., Helgee, B., Olsson, N. (2009) Controllable alignment of nematics by nanostructured polymeric layers. *Liquid Crystals* **36** (6), 747-753.

[10] Lee, H.-J., Kang, D., Clark, C.M., Rosenblatt, C. (2009) Full control of nematic pretilt angle using spatially homogenous mixtures of two polyimide alignment materials. *J. Appl. Phys.* **105** (2), 023508.

[11] Lin, C.-J., Hong, G.-T., Pan, R.-P. (2009) Alignment control of rubbed polyimide layers by UV-irradiation. *Mol. Cryst. Liq. Cryst.* **512**, 911937-911945.

[12] Reznikov, Y., Petschek, R.G., Rosenblatt, C. (1996) Magnetic field-mediated alignment of a nematic liquid crystal at a polymer surface exposed to ultraviolet light. *Appl. Phys. Lett.* **68** (16), 2201-2203.

[13] Seo, D.-S. (1999) Generation of high pretilt angle and surface anchoring strength in nematic liquid crystal on a rubbed polymer surface. *J. Appl. Phys.* **86** (7), 3594-3597.

[14] Seo, D.-S. (2000) Anchoring strength and high pretilt angle in nematic liquid crystal on rubbed organic solvent polyimide surfaces with trifluoromethyl moieties. *J. Korean Phys. Soc.* **36** (1), 29-33.

[15] Vaughn, K.E., Sousa, M., Kang, D., Rosenblatt, C. (2007) Continuous control of liquid crystal pretilt angle from homeotropic to planar. *Appl. Phys. Lett.* **90** (19), 194102.

[16] Wu, W.-Y., Wang, C.-C., Fuh, A.Y.-G. (2008) Controlling pre-tilt angles of liquid crystal using mixed polyimide alignment layer. *Optics Express* **16** (21), 17131-17137.

[17] Yeung, F.S.-Y., Xie, F.-C., Wan, J.T.-K., Lee, F.K., Tsui, O.C.K., Sheng, P., Kwok, H.-S. (2006) Liquid crystal pretilt angle control using nanotextured surfaces. *J. Appl. Phys.* **99** (12), 124506.

[18] Willman, E., Fernandez, F.A., James, R., Day, S.E. (2008) Switching dynamics of a Post Aligned Bistable nematic liquid crystal Device. *J. Disp. Technol.* **4** (3), 276-281.

[19] Stewart, I.W. (2004) The static and dynamic continuum theory of liquid crystals. *Taylor & Francis.*

[20] DeGennes, P.G., Prost, J. (1993) *The Physics of Liquid Crystals (2nd Ed.)* International Series of Monographs on Physics (83), Oxford Science Publications.

[21] Chandrasekhar, S. (1992) *Liquid Crystals* (2nd Ed.), Cambridge University Press.

[22] Blinov, L.M., Kolovsky, M., Nagata, T., Ozaki, M., Yoshino, K. (1999) Influence of guest conformation (rod- or banana-like photo-isomers) on flexoelectric coefficients in nematic liquid crystals. *Jpn. J. Appl. Phys.* **38**, L1042-L1045.

[23] Murthy, P.R.M., Raghunathan, V.A., Madhusudana, N.V. (1993) Experimental determination of the flexoelectric coefficients of some nematic liquid crystals. *Liquid Crystals* **14**, 483-496.

[24] Davidson, A.J., Mottram, N,J. (2002) Flexoelectric switching in a bistable nematic device. *Phys. Rev. E* **65**, 051710.

[25] Rapini, A. & Papoular, M. (1969) Distorsion d'une lamelle nématique sous champ magnétique. Conditions d'ancrage aux parois. *J. Phys. (Paris) Colloq.* **30**, C4, 54-56.

[26] Leslie, F.M. (1979) Theory of flow phenomena in liquid crystals. *Adv. Liquid Crystals* **4**, 1-81.

[27] Kedney, P.J., Leslie, F.M. (1998) Switching in a simple bistable nematic cell. *Liquid Crystals* **24** (4), 613-618.

[28] Cummings, L.J., Richardson, G. (2006) Bistable nematic liquid crystal device with flexoelectric switching. *Europ. J. Appl. Math.* **17**, 435-463.